# Assessment of fatigue and corrosion fatigue behaviours of the nitrogen ion implanted CpTi

CrossMark

Nurdin Ali [a], Mohamad Ali Fulazzaky [b,*], Muhammad Sukri Mustapa [c], Mohd Imran Ghazali [c], Muhammad Ridha [a], Tjipto Sujitno [d]

[a] Department of Mechanical Engineering, Faculty of Engineering, Syiah Kuala University, Banda Aceh 23111, Indonesia
[b] Institute of Environmental and Water Resources Management, Water Research Alliance, Universiti Teknologi Malaysia, 81310 UTM Skudai, Johor Bahru, Johor, Malaysia
[c] Faculty of Mechanical and Manufacturing Engineering, Universiti Tun Hussein Onn Malaysia, 86400 Parit Raja, Batu Pahat, Johor, Malaysia
[d] National Nuclear Energy Agency, Jalan Babarsari PO Box 6101 Ykbb, Yogyakarta 55281, Indonesia

## ARTICLE INFO

## ABSTRACT

The fatigue and corrosion fatigue behaviours of commercially pure titanium (CpTi) have been particularly studied because the requirements of titanium (Ti) base materials are widely used for biomedical applications. The optimal properties of CpTi surface can be preserved by nitrogen ion implantation at a certain dose and energy. Still the fatigue and corrosion fatigue behaviours of nitrogen ion implanted CpTi (Nii-Ti) must be verified. This study performs the fatigue tests for CpTi and Nii-Ti specimens in a laboratory air and the corrosion fatigue tests for Nii-Ti specimens in a saline solution. Effects of nitrogen ion implantation on surface properties can improve the fatigue strength, fatigue life and corrosion fatigue life of Ti base materials. The corrosion pit growth law has been established on the basis of empirical data for predicting the corrosion penetration rate to estimate to the service life of Nii-Ti.

© 2013 Elsevier Ltd. All rights reserved.

## 1. Introduction

Commercially pure titanium (CpTi) is one of the important metallic materials for medical applications due to its characteristics of a combination of high specific strength, excellent corrosion resistance, low temperature ductility and good biocompatibility in human body environment [12,20,22,24,31,35]. It is well known that titanium (Ti) and its alloy are the most attractive metallic materials for biomedical applications owing their low weight-to-volume ratio, high strength-to-weight ratio, high fatigue strength and good corrosion resistance [4,19,29] and could be mainly used as substituting materials for hard tissue replacement [25]. Commonly, grade of CpTi cannot offer the best possible optimisation of an exceptional wear resistance and very acceptable workability when used for artificial joint replacement. Therefore, the modification of CpTi surface is still necessary for enhanced wear resistance and its workability. It is suggested that certain properties of CpTi may change as a consequence of the modification of surface structure. For biomedical applications, the corrosion fatigue behaviours of CpTi caused by combined synergistic actions of cyclic loading and corrosive environment are the important issues.

The treatment of CpTi surface can play a significant role in retarding the initiation and growth of fatigue cracks. Imparting residual compressive stress in surface layers of the metallic components such as by shot-peening [7], anodic oxidation treatment [8], plasma nitriding [14] and sandblasting [20] is one of the ways to improve fatigue strength characteristics. Many studies have been carried out to assess the fatigue and corrosion fatigue behaviours of metallic materials, such as the fatigue behaviours of aluminium alloy and stainless steel both in laboratory air and in a corrosive environment [7], the effect of ion implantation on fatigue life of steel bearing [9], the corrosion fatigue of ion nitride AISI 4140 steel [14], the effects of sandblasting on enhancement of fatigue and corrosion properties of pure Ti [20], the fatigue and cyclic deformation behaviours of surface-modified titanium alloys [24] and the corrosion fatigue life of CpTi and Ti–6Al–4V alloys [35]. Still the fatigue and corrosion fatigue behaviours of nitrogen ion implanted CpTi (Nii-Ti) needs to be verified as a challenging issue to increase its service life in an acidic environment of the human body for biomedical applications.

The objectives of this study are as follows: (1) to verify the surface characteristics of CpTi and Nii-Ti specimens based on the X-ray diffraction (XRD) patterns and tensile and wear resistance properties, (2) to evaluate the fatigue life of CpTi and Nii-Ti from the experiments conducted in laboratory air and corrosion fatigue life of Nii-Ti from the experiments conducted in a saline solution,

* Corresponding author. Tel.: +60 75531702; fax: +60 75531575.
E-mail address: fulazzaky@gmail.com (M.A. Fulazzaky).

and (3) to establish the corrosion pit growth law on the basis of experimental data to be used for determining the corrosion penetration rate in order to estimate the service life of Nii-Ti in an acidic environment.

## 2. Materials and methods

### 2.1. Materials

This study used the CpTi in rod form of grade VT1-0 with a diameter of 30 mm originally delivered from Fiko Ltd. (Kyiv, Ukraine). The CpTi impurity consists of 0.04% N, 0.05% C, 0.003% H, 0.13% Fe, 0.11% O, 0.49% Al, 0.03% S and 0.30% others metals being inherent in its mechanical properties characterised with a tensile strength of 430 MPa, elongation of 29% and reduction area of 56%. Hence, Al is the main impurity element of the CpTi. Fig. 1 shows the surface microstructure of CpTi specimen as an image of its original condition.

### 2.2. Experimental methods

#### 2.2.1. Preparation of the specimens

The CpTi 30 mm diameter rod was cut to have a length of 90 mm using a fully automatic band saw machine (Everising model H-360HA) and machined using a Pinnacle milling machine. This CpTi cylindrical rod (30 mm diameter × 90 mm length) was split into four parts using EDM wire cut machine (Model Mitsubishi RA 90). Then, each part of such split CpTi rod was machined using Harrison M300 Lathe machine to have a smaller CpTi rod of 12 mm diameter and 90 mm length. The precise size and shape (see Fig. 2) of each specimen was made using the CNC machine of Mazak Quick Cut Nexus 100-II for machining precision parts driving the specimen. Note that the values of stress-concentration factor for each specimen are the same to be 1.04 [28]. Each specimen was grounded with silicon carbide abrasive paper and then polished it using a diamond paste of 1 μm to have an achievability of surface roughness values between 0.06 and 0.11 μm. The polished specimen was cleaned by rinsing with water and immersed in ultrasonic cleaner of ethanol for 30 min; it was then dried at room temperature. The ASTM standards E466 and E468 were to be consulted for details of the test for each CpTi base specimen. Fig. 2 shows the size and shape of the specimen according to ASTM E466. Fifteen specimens of original CpTi termed as CpTi were subjected to fatigue test. Thirty specimens were subjected to the implantation of nitrogen ions in optimum dose of $2.0 \times 10^{17}$ ions cm$^{-2}$ and optimum energy of 100 keV [13] and termed as Nii-Ti, where fifteen Nii-Ti
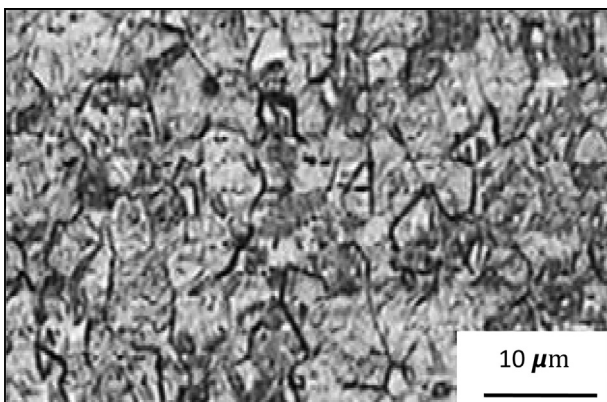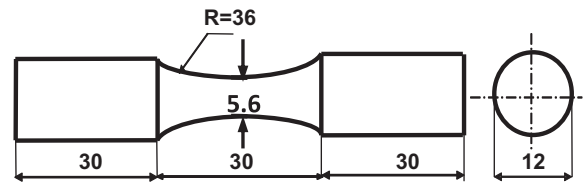
**Fig. 2.** Size and shape (in mm) of the specimen according to ASTM E466.

specimens were used for fatigue test and the remainder of fifteen Nii-Ti specimens were used for corrosion fatigue test.

#### 2.2.2. Fatigue and corrosion fatigue tests

In this study, fatigue testing followed the guidelines of ASTM F 1801-97 [3]. The fatigue tests were performed using a fatigue testing machine (Shimadzu Servopulser of 100-kN capacity) and run on a sophisticated fatigue machine with dedicated software GLUON series dynamic characteristics test package of software version 2.40 2001 where the data processing equipment to be used in the tests has been acquired in connection with a personal computer of Dell Precision T3400. Both fatigue tests of fifteen CpTi and fifteen Nii-Ti specimens were conducted at a stress ratio, $R = -1$, by tension–compression in laboratory air and carried out as follows: (1) at a frequency of 10 Hz for applied stresses of 300 and 320 MPa in order to have a chance of avoiding temperature rises and (2) at a frequency of 20 Hz for applied stresses of 290 MPa and below.

In a previous study on corrosion-fatigue life of CpTi and Ti–6Al–4V alloys in different storage environments by Zavanelli et al. [35] has reported that the fatigue life was significantly reduced because of the production of corrosion pits caused by superficial reactions. In the present work, every Nii-Ti specimen was soaked with a saline solution of 0.9% NaCl, wrapped around the gage section of fatigue corrosion test specimen, and sealed with tape and a plastic film to avoid evaporation. The updated model of corrosion chamber (see Fig. 3) was specially designed for evaluating the corrosion fatigue behaviour of surface treatment for Nii-Ti specimen. Saline solution was pumped at a flow rate of 500 mL mn$^{-1}$ through a fluid pump to provide a fresh supply of corrosive solution to the specimen at room temperature. Aerator provides a constant source of oxygen as it pulls air from its surrounding to aerate saline solution
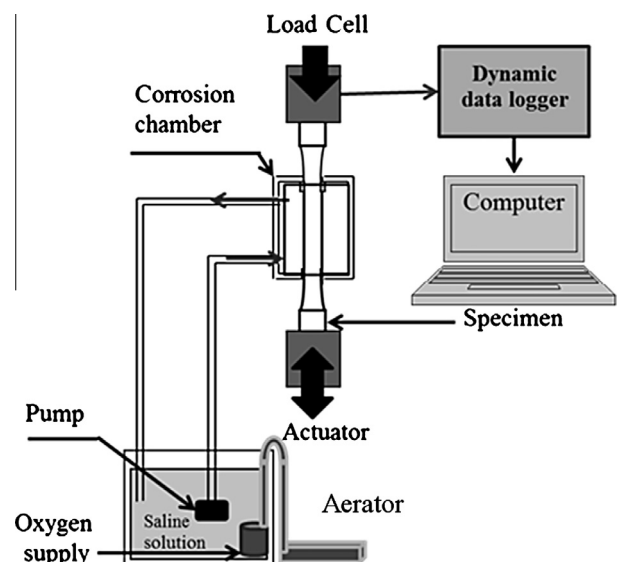
**Fig. 1.** Surface microstructure of the CpTi specimen as an image of its original condition.

**Fig. 3.** Schematic of the corrosion fatigue test technique.

through a diffuser ball. Even though the rotating bending fatigue tests in the previous studies [17,28] were carried out under cyclic speed of 30 Hz, the corrosion fatigue tests to fifteen Nii-Ti specimens for all applied stresses were conducted at a frequency of 20 Hz and at a stress ratio, $R = -1$, by tension–compression in a saline solution. Three Nii-Ti specimens were chosen to study the corrosion behaviours of current density and corrosion potential during corrosion fatigue where the measurements to follow the method proposed by Fulazzaky et al. [13] were carried out using a potentiostat (model: WPG 100, WonATech Instrument). The potentiodynamic polarisation curves of corrosion potential ($E_{corr}$) versus logarithm of corrosion current density ($i_{corr}$) were measured using a potentiostat of "WPciPG English Version 1.11" and controlled using a personnel computer with dedicated software of "IVMAN 1.0.015" for potentiodynamic analysis. The potentiodynamic polarisation curves were recorded by scanning the electrode potential from −500 mV to 1500 mV (vs SCE) with a scanning rate of 5 mV s$^{-1}$.

### 2.2.3. Fatigue fracture surface scanning

In this study, three specimens were used for the assessment of fatigue fracture surface, such that: (1) the CpTi specimen was initially tested with an applied stress of 260 MPa in laboratory air, (2) the Nii-Ti specimen was initially tested with an applied stress of 280 MPa in laboratory air, and (3) the Nii-Ti specimen was initially tested with an applied stress of 280 MPa in a saline solution. The penetration rate of Nii-Ti might be estimated from the change in corrosion behaviours. Critical fatigue cracks and their sizes were evidenced by striations on fatigue fracture surfaces. Fracture surfaces of CpTi and Nii-Ti were examined by Scanning Electron Microscopy (SEM) (Model JSM-6380 LA from JEOL, Japan) and critical cracks on fracture surfaces of CpTi and Nii-Ti specimens were observed at a selected stress level.

## 3. Results and discussion

### 3.1. Surface characteristics

In a previous study by Fulazzaky et al. [13] has reported that the optimum properties of Nii-Ti surface have a surface hardness of 212 HV and a corrosion rate of 0.0040 mm y$^{-1}$ for nitrogen ion implanted at 100 keV with a dose of $2.0 \times 10^{17}$ ions cm$^{-2}$. The corrosion rates of Nii-Ti in a saline solution and in a simulated body fluid as high as 0.0040 and 0.0014 mm y$^{-1}$, respectively, have also been reported [13]. The XRD analysis can be a very straightforward and easy to use method to determine the change in surface structure of Ti base materials due to formation of TiN and Ti$_2$N phases in the form of compound layer. Fig. 4 shows the XRD pattern of CpTi

and Nii-Ti implanted with a dose of $2.0 \times 10^{17}$ ions cm$^{-2}$ at 100 keV. The unit cell for nitride phases was verified using the grazing incidence X-ray diffraction (GXRD) that crystal structure of TiN phase is face-centered cubic (fcc) lattice with $a = 0.4241$ nm and that of Ti$_2$N phase is body-centered tetragonal (bct) lattice with $a = 0.4945$ nm and $c = 0.3034$ nm. The complex microstructures with deeply etched grain boundaries and nano-sized asperities formed nitride phases are the important factors for improving adhesive strengths of films deposited on Ti base materials [15].

### 3.2. Mechanical properties

The results of the measurement of tensile properties (Fig. 5a) shows that the increases of ultimate tensile strength, yield strength (at 0.2% offset) and tensile elongation 12.5% (25 mm gage length) as high as 42 MPa i.e., from 497 MPa (CpTi) to 539 MPa (Nii-Ti), 18 MPa i.e., from 402 MPa (CpTi) to 420 MPa (Nii-Ti) and 3% i.e., from 34% (CpTi) to 37% (Nii-Ti), respectively, were verified. The specimen of Nii-Ti shows better mechanical behaviour with better tensile properties than the specimen of CpTi and is promising candidate for load bearing applications as implant materials [6]. Pin-on-disc wear tests using the computerised pin-on-disc wear testing machine (DUCOM: TR 20LE, Bangalore, India) have to do with previous work experience [1] were conducted under dry sliding conditions on both the specimens of CpTi and Nii-Ti, after various melt treatments at a fixed load of 5 N and a constant sliding speed of 1.25 m s$^{-1}$ and at varying sliding distances from 1 to 7 km at room temperature (see Fig. 5b). A high carbon alloy steel (EN-31 steel) with a surface hardness of 698 HV (HRC 56-60) was used as solid surface countertop. Wear samples were cleaned with acetone and weighed to an accuracy of ±0.001 g prior to testing at 30 mn intervals during the test. It is recognised that the volume loss offers a truer picture than weight loss, particularly when comparing wear resistance properties of metallic materials with large differences in density. The volume of the lost material for CpTi and Nii-Ti specimens was calculated dividing the mass loss value by Ti density. Note that density of Ti is 4507 kg m$^{-3}$. Fig. 5b shows that the volume loss at a sliding distance of 6.8 km decreases from 30.8 mm$^3$ for CpTi to 21.2 mm$^3$ for Nii-Ti specimen caused by the change in surface properties.

### 3.3. Fatigue and corrosion fatigue life

The experiments of fatigue tests in laboratory air were carried at stress levels ranging between 240 and 320 MPa in order to assess fatigue properties of fifteen CpTi and fifteen Nii-Ti specimens. Fig. 6 shows the test results in data presented as a plot of stress ($S$) against the number of cycles to failure ($N$), which is known as an $S$–$N$ curve. Note that $N$ is the average value of cyclic loading to a stress level. The $S$–$N$ curve for CpTi specimen (**2**, red) is very similar to that obtained by Fleck and Eifler [11] (**1**, black) (see Fig. 6a). The figure shows the trend of decreasing $S$ as the value of $N$ increases. The fatigue life of Nii-Ti (green) could be slightly greater than that of CpTi (red) specimen at a high stress level of 320 MPa; however, -it has a clear difference between Nii-Ti (green) and CpTi (red) at low stress levels ranging between 260 and 300 MPa (see Fig. 6a), indicating that the value of $N$ for Nii-Ti is much more than that for CpTi specimen at the same $S$ value. At $N = 10^7$ cycles, the fatigue strengths of CpTi (red) and Nii-Ti (green) specimen as high as 250 and 260 MPa, respectively, were verified, hence the nitrogen ion implantation effects on micro-hardness properties of CpTi can cause a significant increase in yield strength of 10 MPa. As a conclusion, the use of nitrogen ion implantation may be a good technique for the improvement of fatigue strength of Ti base materials.
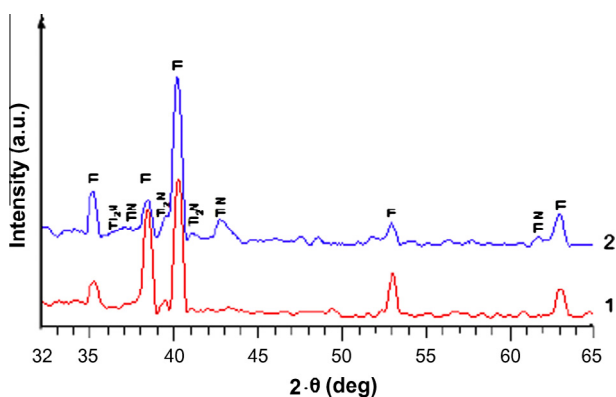


**Fig. 4.** The XRD pattern for: (1) CpTi specimen and (2) Nii-Ti specimen.
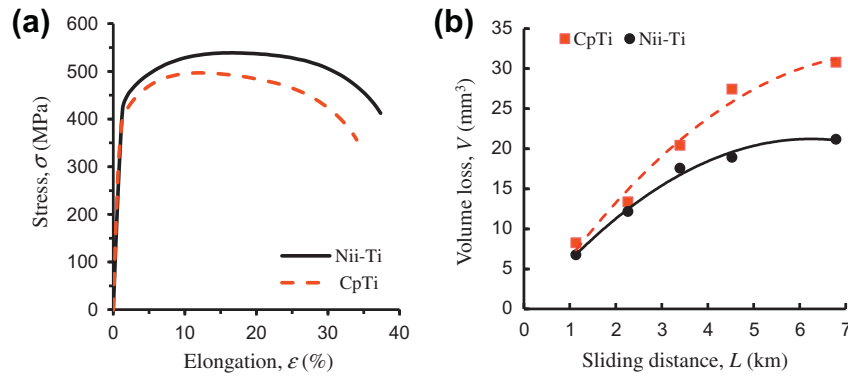
**Fig. 5.** Mechanical behaviours of CpTi and Nii-Ti specimens; (a) $\sigma$–$\varepsilon$ curve and (b) $V$–$L$ curve.
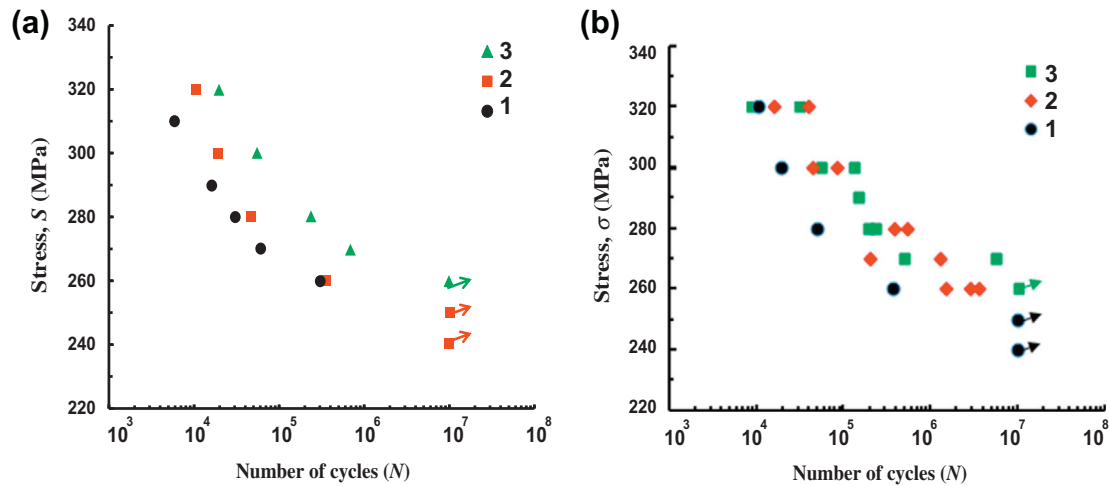


**Fig. 6.** *S–N* curves: (a) to assess the fatigue properties with **1**: the results for CpTi specimen from Fleck and Eifler [11], **2**: the results for CpTi specimen and **3**: the results for Nii-Ti specimen and (b) to assess the fatigue and corrosion fatigue properties with **1**: the results for CpTi specimen tested in laboratory air, **2**: the results for Nii-Ti specimen tested in a saline solution and **3**: the results for Nii-Ti specimen tested in laboratory air.

The data (Fig. 6b) obtained from the experiments in laboratory air (i.e., six CpTi and ten Nii-Ti specimens) and the experiments in a saline solution of 0.9% NaCl (i.e., eleven Nii-Ti specimens) at stress levels ranging between 240 and 320 MPa were used to assess the fatigue and corrosion fatigue properties. Note that corrosion fatigue occurs by the combined synergistic actions of cyclic loading and a corrosive environment [21,34]. The experiments for fatigue tests in laboratory air were subjected to the test specimens conducted at a set of high stress amplitudes and a low frequency of 10 Hz so as to avoid overheating. Fig. 6b shows the trends in fatigue *S–N* curve for the specimens of CpTi tested in laboratory air (**1**, black), the specimens of Nii-Ti tested in a saline solution (**2**, red) and the specimens of Nii-Ti tested in laboratory air (**3**, green). At a high stress amplitude (320 MPa), the decrease in fatigue life is not significantly different between corrosion fatigue properties (**2**, red) and fatigue properties (**3**, green). Experimental data verification (Fig. 6b) shows that the N values of fatigue and corrosion fatigue failure as high as 30,336 and 39,427 cycles, respectively, were verified. At a low stress amplitude (260 MPa), the fatigue life of Nii-Ti is better than its corrosion fatigue life, indicating that the N values for Nii-Ti specimens tested in laboratory air (**3**, green) are greater than those tested in a saline solution (**2**, red). The verification of a fatigue endurance limit would not appear to be answerable merely by conducting fatigue test to Nii-Ti specimen (**3**, green) at a low stress level of 260 MPa. The corrosion fatigue life of Nii-Ti (**2**, red) seems better than fatigue life of CpTi (**1**, black)

because the resistance of Nii-Ti in a corrosive environment to repeated loads (cycling) was verified much more important than that of CpTi in laboratory air.

### 3.4. Fatigue fracture surface analysis from the SEM images

The SEM images of CpTi specimen fractured surface tested at 260 MPa in laboratory air are presented in Fig. 7(a–c). The image (see Fig. 7b) shows that crack initiation near the coil line is marked by rough surface; therefore, -the dashed lines indicate a potential crack propagation direction parallel to dimpled lines on the CpTi specimen surface in contrast with the large plains of the smooth surface. The specimen exhibited fracture behaviour of CpTi could easily be identified by observation of the different enlargements of the image. Fig. 7a shows that the crack lengths range from zero to one-half the specimen diameter. The general experience (see Fig. 7b) shows that the cracked initiation results from the concentration of CpTi deformation occur in a small field of finite dimension. The SEM fractograph (see Fig. 7c) shows the transgranular cleavage crack initiation and propagation characteristics for the CpTi specimen. The SEM images of Nii-Ti specimen fractured surface tested at 280 MPa in laboratory air are presented in Fig. 7(d–f). Such a SEM fractograph (see Fig. 7d) can be a valuable way of presenting information which no clearly shows a surface fracture of the Nii-Ti specimen, because of the formation of nitride phase in atomic layer deposition can improve the fatigue
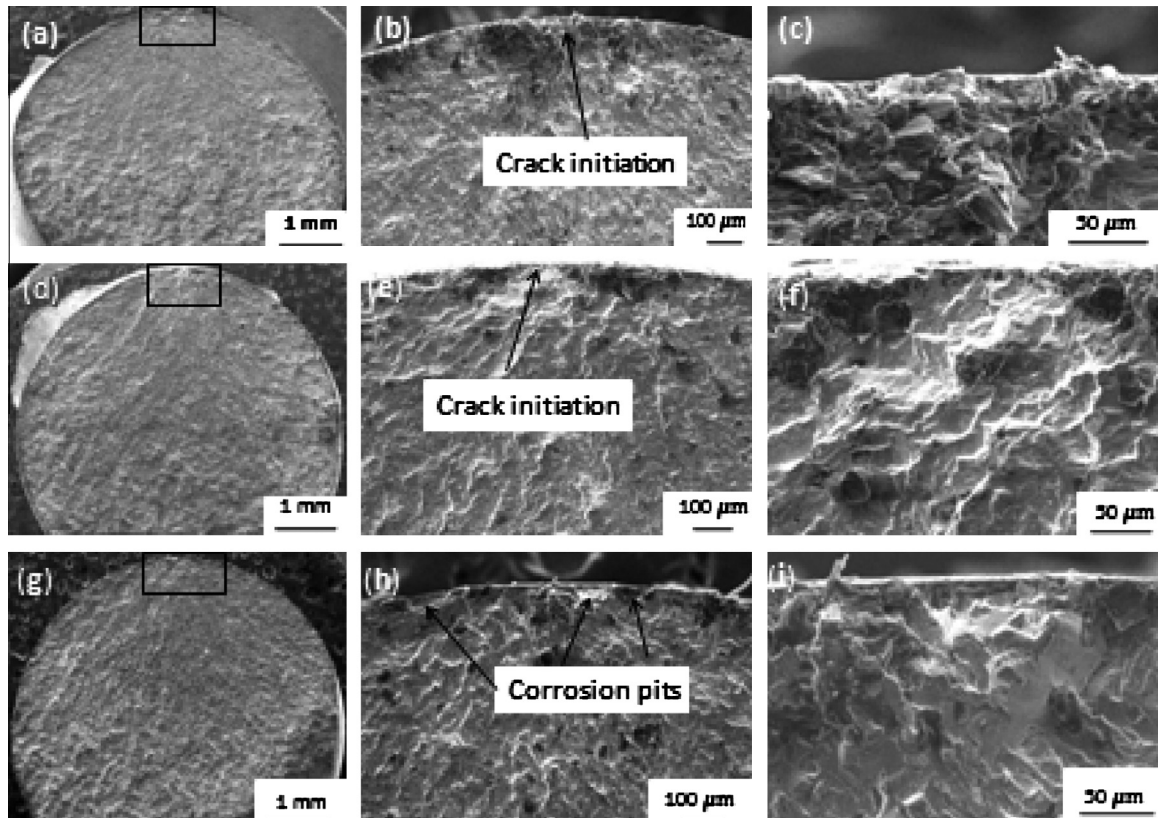
**Fig. 7.** SEM images for: (a–c) CpTi specimen fractured surface tested at 260 MPa in laboratory air, (d–f) Nii-Ti specimen fractured surface tested at 280 MPa in laboratory air and (g–i) Nii-Ti specimen fractured surface tested at 280 MPa in a saline solution.

properties of the specimen. Still, the enlargement of figures (see Fig. 7(e and f)) shows the rough region of the fracture surface with clear evidences of transgranular cracking and the formation of well-defined striations. It is suggested that the reciprocal lattice of fcc and bct structures plays a fundamental role in prolonging fatigue life of the Nii-Ti specimen. The SEM images of corrosion fatigue fracture for the Nii-Ti specimen fractured surface tested at 280 MPa in a saline solution are presented in Fig. 7(g–i). The images show that crack propagation area of the Nii-Ti specimen tested in saline solution (see Fig. 7h) is almost similar to that of the Nii-Ti specimen tested in laboratory air (see Fig. 7e). The initiation of a pit might occur when electrochemical breakdown exposes a small local site on the Nii-Ti surface to damaging species of chloride ions. The pit grows if the high current density involved in the repassivation process does not prevent the formation of a large local concentration of Ti ions produced by dissolution at the point of initiation. Fractal character of fracture surfaces (see Fig. 7h) for the Nii-Ti specimen is marked by the presence of corrosion pits as the starting point of crack propagation and final fracture. Many corrosion pits were created by the salt fog while their diameters ranged between 30 and 80 µm [5]. The uniform corrosion results from the sites, not necessarily fixed in a location, that are distributed over the Nii-Ti surface where the anodic and cathodic reactions take place. The uniform corrosion damage can be manifested in the progressive thinning of a Nii-Ti part until it virtually dissolves away or becomes a delicate lace-like structure. The formation of nitride phases can improve the tensile strength characteristics and elasticity of Nii-Ti specimen, blocking surface deformation and migration of Ti ions into saline solution. In addition, the effect of nitrogen ion implantation on the surface properties caused by passivation due to better electrochemical stability during electrolysis can increase the corrosion fatigue life of Nii-

Ti. Quantification of fracture properties and microstructural features of three specimens by image analysis [32] can explain why the Nii-Ti specimens have a longer fatigue life and corrosion fatigue life than fatigue life of the CpTi specimen.

### 3.5. Corrosion pit growth law

Since most corrosion reactions occurring in the presence of a liquid, such as a saline solution of 0.9% NaCl, are not chemical but are electrochemical [26], the use of chemical equilibrium is of minimal use for studying corrosion in acidic environments. A useful way to study the relation of potential failure to corrosion is through the use of an electrochemical method. In this study, the effect of a cyclic stress on pit initiation and growth processes was evaluated for the corrosion fatigue of Nii-Ti specimen. The cause of potential failure by corrosion penetration rate was investigated using electrochemical method, which offers a simple method to characterise the corrosion fatigue behaviour of Nii-Ti in aqueous electrolytes when comparing with other methods proposed in the previous studies [18,28]. The penetration is uniform or even across the specimen surface [27]. The maximum penetration rate not the average penetration rate may imply potential failure whereas the average penetration rate would not [23]. Fig. 8 shows the potentiodynamic polarisation curves of plotting the corrosion potential ($E_{corr}$) versus log corrosion current density ($i_{corr}$) for Nii-Ti specimen measured in a freshly aerated 0.9% NaCl solution at 260 MPa with the elapsed times ($t$) of 0, 4 and 40 h. The figure shows that $E_{corr}$ decreases slightly from −342 to −373 to −378 mV but $i_{corr}$ increases from 60 to 193 to 740 nA as $t$ increases from 0 to 4 to 40 h, respectively. The curves were affected by a phenomenon known as passivation. Passivation can occur only in certain conditions and, at $t$ = 0 h, is clearly visible in curve with
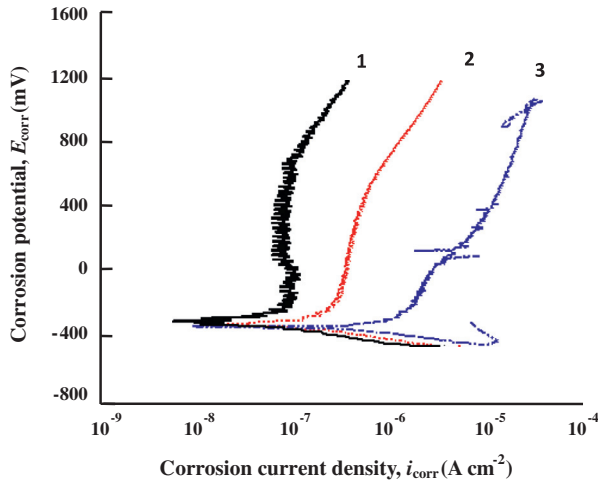
**Fig. 8.** Potentiodynamic polarisation curves measured at 260 MPa with the different elapsed times of 0 h (1, black), 4 h (2, red) and 40 h (3, blue). (For interpretation of the references to colour in this figure legend, the reader is referred to the web version of this article.)

convex left side (**1**, black). The underlying mechanism of Nii-Ti surface passivation as obtained by nitrides formation appears slightly flat with a noticeable left-convex curve at $t = 4$ h (**2**, red) and, at $t = 40$ h, is not visible in curve with negative convexity (**3**, blue). The passivation mechanism and passive state stability are considered to relate to the manner in which undissociated NaCl molecules can immediately participate during the corrosion process. The sluggish kinetics of molecular oxygen at low current density could potentially result in a slight increase in $E_{corr}$ (see Fig. 8).

In this study, the power regression takes the input signal of penetration rate ($P_r$) and fits a function to $t$ where $t$ is the variable along the horizontal axis. Fig. 9a shows that the log–log graph of plotting $P_r$ versus $t$ gives a trend line in its good fit correlation ($R^2 > 0.885$; see Caption of Fig. 9a). Therefore, the power equation to calculate $P_r$ during the corrosion process can be written as follows:

$$P_r = \eta \times t^{\alpha} \tag{1}$$

where $P_r$ is penetration rate at Nii-Ti specimen during the corrosion process (in $\mu$m y$^{-1}$), $\eta$ is penetration rate index of dependence on applied stress amplitude (in $\mu$m h$^{-2}$), $t$ is elapsed time (in h) and $\alpha$ is experimental determined parameter (dimensionless).

The power equation (see Eq. (1)) gives a conditional expected value of $\alpha = 0.78$ (the average rounded value; see Caption of Fig. 9a) and index $\eta$ variable; therefore, -the values of $\eta$ were verified to increase from 0.1423 to 0.2944 to 0.7604 $\mu$m h$^{-2}$ as the stress level increases from 250 to 260 to 280 MPa, respectively. The degree of corrosion damage can depend on several factors, including the nature of the event and the force of impact [2,33]. Susceptibility to intergranular corrosion depends on the environment and on the extent of intergranular precipitation, which is a function of alloy composition, fabrication and heat treatment parameters. The effect of penetration rate of molecular oxygen on the Nii-Ti subsurface depends on its diffusion characteristics and varies from stress to stress amplitude. The increase in resistance can be related directly to Ti loss and the Ti loss as a function of t is by definition the corrosion rate. A plot (Fig. 9b) of $\eta$ versus $\sigma$ can yield a linear trend line in its good fit correlation ($R^2 > 0.99$; see caption of Fig. 9b) and gives the mathematical expression that,

$$\eta = a \times \sigma - b \tag{2}$$

By substituting Eq. (2) into Eq. (1) yields,

$$P_r = (a \times \sigma - b) \times t^{\alpha} \tag{3}$$

where $P_r$ is penetration rate for Nii-Ti specimen during the corrosion process (in $\mu$m y$^{-1}$), $a$ is crack propagation coefficient (in $\mu$m MPa$^{-1}$ h$^{-2}$), $\sigma$ is stress amplitude (in MPa), $b$ is corrosion penetration rate constant (in $\mu$m h$^{-2}$), $t$ is elapsed time (in h) and $\alpha$ is experimental determined parameter (dimensionless).

The corrosion rate expressed as a penetration rate is calculated from the corrosion current density using Faraday's law as $P_r = 3.27 \times (i_{corr}/d) \times (W/n)$ where $P_r$ is the penetration rate (in $\mu$m y$^{-1}$), $i_{corr}$ is the corrosion current density (in $\mu$A cm$^{-2}$), $d$ is the density (in g cm$^{-3}$), $W$ is the atomic weight (dimensionless), and $n$ is the number of electrons transferred to oxidise an atom. For pure Ti, $d = 4.507$ g cm$^{-3}$ and $W = 47.867$. In this study, only four-valent corrosion products of TiO$_2$ were considerably formed during the corrosion process, hence the only $n = 4$ should be used for determining the values of $P_r$. The estimation of corrosion fatigue life is based on the assumptions that: (1) a corrosion pit (see Fig. 7h) may be modelled by an equivalent semielliptical surface crack and (2) the aspect ratio (pit depth/pit width) of formed pit that gives an indication of the profile of the defect would remain constant during the corrosion process. Because the values of $a$, $b$ and $\alpha$ in Eq. (3) are constant, the corrosion pit growth and corrosion fatigue cracking could be considered as time dependent phenomena [10,16]. Typical response by $P_r$ to the instance of crack initiation can be evaluated using a corrosion pit growth rate model
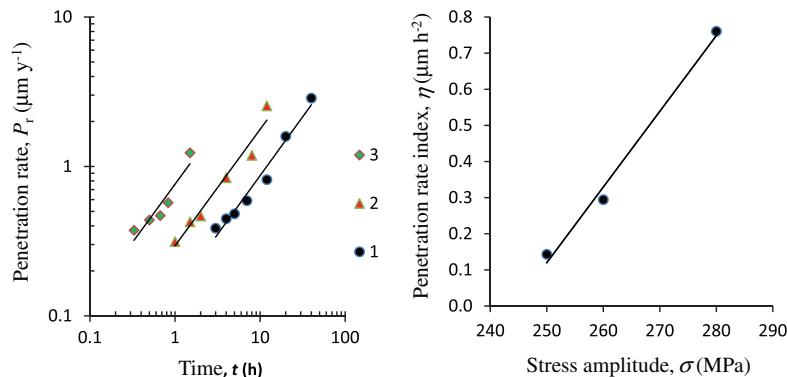


**Fig. 9.** Graphs to predict the corrosion fatigue life of Nii-Ti specimen; (a) the log–log graph of plotting $P_r$ versus $t$ with: (**1**, black) an applied stress of 250 MPa, $\eta = 0.1423$ $\mu$m h$^{-2}$ $\alpha = 0.7811$ and $R^2 = 0.9736$; (**2**, red) an applied stress of 260 MPa, $\eta = 0.2944$ $\mu$m h$^{-2}$ $\alpha = 0.7793$ and $R^2 = 0.9621$; and (**3**, green) an applied stress of 280 MPa, $\eta = 0.7604$ $\mu$m h$^{-2}$ $\alpha = 0.7791$ and $R^2 = 0.8851$, and (b) the linear graph of plotting $\eta$ versus $\sigma$ with $a = 0.021$ $\mu$m MPa$^{-1}$ h$^{-2}$ and $b = 5.121$ $\mu$m h$^{-2}$ and $R^2 = 0.9908$. (For interpretation of the references to colour in this figure legend, the reader is referred to the web version of this article.)

as formulated in Eq. (3). Modelling shows that $P_r$ can be accelerated by increasing either $\sigma$ or $t$. The model accounts for ion implantation energy and dosage, crack propagation and stress amplitude in order to assess the impact of corrosion pit growth on the remaining service life of Nii-Ti. Estimation of the corrosion fatigue life of Nii-Ti on the basis of corrosion pit growth law can be expressed as $P_r = (0.021 \times \sigma - 5.121) \times t^{0.78}$. This expression fits the experimental data well ($R^2 = 0.9908$; see caption of Fig. 9b) in describing the initiation and growth of a fatigue crack emanating from a pit, rather than the estimation of corrosion cavity growth rate for service life of Nii-Ti. According to the corrosion pit growth law, the corrosion penetration rate tends to slow to a much greater extent with exposure time than the mass loss rate [30], because of $\alpha = 0.78$ is less than one.

## 4. Conclusions

This study performed the fatigue and corrosion fatigue tests for CpTi and Nii-Ti specimens. The fatigue fracture surface was analysed from the SEM images. Effects of nitrogen ion implantation on surface properties and adhesion strength of nitride films can increase the fatigue and corrosion fatigue life of Nii-Ti. The fatigue endurance limit of Nii-Ti specimens tested in a saline solution would not appear by conducting the fatigue tests at low stress amplitude. The SEM image analysis to indicate fatigue fracture surface of Nii-Ti tested in laboratory air and in a saline solution at 280 MPa that could initiate a fatigue crack appears to be unclear; however, -it is clear that the crack initiation appears for CpTi specimen even the fatigue test was conducted at 260 MPa in laboratory air. The penetration rate of the Nii-Ti is mainly affected by stress amplitude and time and can be estimated by using the corrosion pit growth law $P_r = (0.021 \times \sigma - 5.121) \times t^{0.78}$. The corrosion pit growth law for Nii-Ti was established for contribution to the service life estimation of Ti base materials in acidic environments.

## Acknowledgements

## References

[1] Agung I, Syarif J, Ghazali MJ, Sajuri Z. Effect of Cu particles on wear behaviour of Fe–3mass%Cu under dry sliding condition. Key Eng Mater 2011;462–463:1224–9.

[2] Akop'yan VA, Rozhkov YeV, Shevtsov SN. Correlations between parameters of acoustic-emission signals and corrosion damage in aluminum alloys. Russ J Nondestruct Test 2007;43:390–6.

[3] ASTM Standard, ASTM., 2010. Standard practice for corrosion fatigue testing of metallic implant materials. Annual book of ASTM standard, ASTM standard F1801-97. ASTM International.

[4] Balazic M, Kopac J, Jackson MJ, Waqar A. Review: titanium and titanium alloy applications in medicine. Int J Nano Biomater 2008;1:3–34.

[5] Bathias C, Palin-Luc T. Exploration of the corrosion fatigue of steel in the gigacycle regime for oil industry. AFA workshop: fitness for service in chemical industries. Aswan (Egypt); November 2012. p. 25–27.

[6] Bolzoni L, Weissgaerber T, Kieback B, Ruiz-Navas EM, Gordo E. Mechanical behaviour of pressed and sintered CP Ti and Ti–6Al–7Nb alloy obtained from master alloy addition powder. J Mech Behav Biomed Mater 2013;20:149–61.

[7] Cheong KC, Nam JH, Lee JH, Kim TH. Effects of shot-peening on the corrosion fatigue life of Al 7075-T6. In: Proc. of the 9th International Conference on Shot Peening, 2005. p. 338–43.

[8] Cirik E, Genel K. Effect of anodic oxidation on fatigue performance of 7075-T6 alloy. Surf Coat Technol 2008;202:5190–201.

[9] Dodd A, Kinder J, Torp B, Nielsen BR, Rangel CM, Da Silva MF. The effect of ion implantation on the fatigue life and corrosion resistance of M50 steel bearings. Surf Coat Technol 1995;74–75:754–9.

[10] Eliaz N, Shachar A, Tal B, Eliezer D. Characteristics of hydrogen embrittlement, stress corrosion cracking and tempered martensite embrittlement in high-strength steels. Eng Fail Anal 2002;9:167–84.

[11] Fleck C, Eifler D. Corrosion, fatigue and corrosion fatigue behaviour of metal implant materials, especially titanium alloys. Int J Fatigue 2010;32:929–35.

[12] Fokumoto S, Tsubakino H, Terasawa M, Mitamura T, Nakamura K, Okazaki Y. Corrosion resistance of nitrogen ion implanted titanium alloy for medical implants in physiological saline solution. In: Conference on Ion Implantation Technology. Aplbach, 17–22 September 2000, IEEE explore, p. 777–80.

[13] Fulazzaky MA, Ali N, Samekto H, Ghazali MI. Assessment of CpTi surface properties after nitrogen ion implantation with various doses and energies. Metall Mater Trans A 2012;43:4185–93.

[14] Genel K, Demirkol M, Gülmez T. Corrosion fatigue behaviour of ion nitrided AISI 4140 steel. Mater Sci Eng A 2000;288:91–100.

[15] Hieda J, Niinomi M, Nakai M, Cho K, Gozawa T, Katsui H, et al. Enhancement of adhesive strength of hydroxyapatite films on Ti–29Nb–13Ta–4.6Zr by surface morphology control. J Mech Behav Biomed Mater 2013;18:232–9.

[16] Hoeppner DW, Arriscorreta CA. Exfoliation corrosion and pitting corrosion and their role in fatigue predictive modeling: state-of-the-art review. Int. J Aerosp Eng; 2012, Article ID 191879.

[17] Ishihara S, Saka S, Nan ZY, Goshima T, Shibata H, Ding BL. Study on the pit growth during corrosion fatigue of aluminum alloy. Int J Mod Phys B 2006;20:3975–80.

[18] Ishihara S, Saka S, Nan ZY, Goshima T, Sunada S. Prediction of corrosion fatigue lives of aluminum alloy on basis of corrosion pit growth law. Fatigue Fract Eng Mater Struct 2006;29:472–80.

[19] Jagielski J, Piatkowska A, Aubert P, Thome L, Turos A, Abdul Kader A. Ion implantation for surface modification of biomaterials. Surf Coat Technol 2006;200:6355–61.

[20] Jiang XP, Wang XY, Li JX, Li DW, Man C-S, Shepard MJ, et al. Enhancement of fatigue and corrosion properties of pure Ti by sandblasting. Mater Sci Eng A 2006;429:30–5.

[21] Khan Z. Effect of corrosive environment on the fatigue crack initiation and propagation behavior of Al 5454–H32. J Mater Eng Perform 1996;5:78–83.

[22] Koike M, Fujii H. The corrosion resistance of pure titanium in organic acids. Biomaterials 2001;22:2931–6.

[23] Lambers H-G, Rüsing CJ, Niendorf T, Geissler D, Freudenberger J, Maier HJ. On the low-cycle fatigue response of pre-strained austenitic $Fe_{61}Mn_{24}Ni_{6.5}Cr_{8.5}$ alloy showing TWIP effect. Int J Fatigue 2012;40:51–60.

[24] Leinenbach C, Eifler D. Fatigue and cyclic deformation behaviour of surface-modified titanium alloys in simulated physiological media. Biomaterials 2006;27:1200–8.

[25] Liu X, Chu PK, Ding C. Surface modification of titanium, titanium alloys, and related materials for biomedical applications. Mater Sci Eng R: Rep 2004;47:49–121.

[26] Long J, Li X, Guo B, Wang L, Zhang N. Catalytic delignification of sugarcane bagasse in the presence of acidic ionic liquids. Catal Today 2013;200:99–105.

[27] Mitra S, Prajapati PK, Shukla VJ, Ravishankar B. Impact of Bhavana Samskara on physico-chemical parameters with special reference to Gandhaka Rasayana prepared by different media and methods. Ayu 2010;31:382–6.

[28] Nan ZY, Ishihara S, Goshima T. Corrosion fatigue behaviour of extruded magnesium alloy AZ31 in sodium chloride solution. Int J Fatigue 2008;30:1181–8.

[29] Niinomi M. Mechanical properties of biomedical titanium alloys. Mater Sci Eng A 1998;243:231–6.

[30] Ricker RE. Analysis of pipeline steel corrosion data from NBS (NIST) studies conducted between 1922 and1940 and relevance to pipeline management. J Res Natl Inst Stand Technol 2010;115:373–92.

[31] Sundararajan T, Praunseis Z. The effect of nitrogen-ion implantation on the corrosion resistance of titanium in comparison with oxygen- and argon-ion implantations. Mater Technol 2004;38:19–24.

[32] Varela P, Aguilera JM, Fiszman S. Quantification of fracture properties and microstructural features of roasted Marcona almonds by image analysis. LWT Food Sci Technol 2008;41:10–7.

[33] Vorobeikov AM, Gorodetskil VA. Evaluation of the degree of corrosion damage of thin-walled structural elements by the punching method. Mater Sci 1975;9:215–7.

[34] Weng L, Zhang J, Kalnaus S, Feng M, Jiang Y. Corrosion fatigue crack growth of AISI 4340 steel. Int J Fatigue 2013;48:156–64.

[35] Zavanelli RA, Pessanha Henriques GE, Ferreira I, De Almeida Rollo JM. Corrosion-fatigue life of commercially pure titanium and Ti–6Al–4V alloys in different storage environments. J Prosthet Dent 2000;84:274–9.